JOURNAL OF THERMOPHYSICS AND HEAT TRANSFER
Vol. 13, No. 1, January–March 1999

Heat Transfer Distributions on a Cylinder with Simulated Thermal Barrier Coating Spallation

Srinath V. Ekkad* and Je-Chin Han†
Texas A&M University, College Station, Texas 77843-3123

Detailed heat transfer distributions are presented over a turbine blade leading-edge model with simulated thermal barrier coating spallation. The blade leading-edge region is simulated by a cylinder in a crossflow with a tailboard. The heat transfer measurements are presented only on one side of the front half of the cylinder. The simulated spallation cavities are rectangular in shape and have rounded corners. The effect of a spallation cavity is studied at four different locations (0–20, 10–30, 20–40, and 35–55 deg). Two different cavity depths are studied at each location to understand the effect of spallation depth on local heat transfer distributions. The effect of freestream turbulence on detailed heat transfer is also presented for each case. Detailed heat transfer measurements are obtained using a transient liquid crystal technique. Detailed heat transfer distributions present the local high-heat transfer and low-heat transfer regions inside and outside the spallation. Results show that spallations can enhance heat transfer up to two times compared with that for a smooth surface. Results also show that the spallation location and depth have a strong effect on local heat transfer distributions on the leading edge. An increase in freestream turbulence further increases the heat transfer coefficients caused by the spallation.

Nomenclature

b = bar grid width, cm
D = cylinder model diameter, cm
h = heat transfer coefficient with spallation, W/m^2-K
h_0 = heat transfer coefficient on a smooth surface, W/m^2-K
k = thermal conductivity of test surface material, W/m-K
k_{air} = thermal conductivity of air, W/m-K
Nu = Nusselt number based on cylinder diameter, hD/k_{air}
Re = Reynolds number based on incident mainstream velocity, $U_\infty D/\nu$
T_i = initial temperature of test surface, °C
Tu = streamwise turbulence intensity, $(\bar{u'^2})^{0.5}/U_\infty$
T_w = liquid crystal temperature at red color change, °C
T_∞ = mainstream temperature, °C
t = time of liquid crystal color change, s
U_∞ = incident mainstream velocity, m/s
u' = local streamwise fluctuating velocity, m/s
X = axial distance measured from grid, cm
Z = spanwise distance, cm
α = thermal diffusivity of test surface material, m^2/s
θ = angle from stagnation
ρ = incident mainstream density, kg/m^3

Introduction

HIGHER inlet temperatures in modern gas-turbine engines provide higher power output and higher thermal efficiency. High-temperature gases have a damaging effect on hot gas path components in the engine. Thermal barrier coatings (TBC) are used to protect engine component metal surfaces from these high-temperature gases. The TBC coating is a heat-resistant ceramic layer sprayed onto the hot gas side of the turbine airfoil. The TBC application process is either done by air plasma spraying (APS) or the plasma vapor deposition (PVD) technique. The TBCs consist of two layers and involve a base bond coat layer applied onto the metal surface and a ceramic top layer applied on top of the base bond. The TBC forms an insulating layer between the hot gases and the airfoil metal surface, reducing the heat input to the airfoil. In land-based gas-turbine engines, the TBC surface undergoes more severe erosion as a result of the use of coal-derived fuels for combustion. When the TBC surface gets damaged, the bond will disassociate and a spallation is formed exposing the inner metal surface to the hot gases. Typically, the heat transfer coefficient around the exposed metal surface area will be enhanced because of tripping of the boundary layer. The enhanced heat transfer coefficients increase heat loads around the spallation, which may be detrimental to the life of the component. The increased heat load will cause further degradation of the spalled region and, hence, will lead to early failure of the turbine component. The present study focuses on the effect of simulated TBC spallation on the leading-edge region of a turbine blade. Watt et al.[1] and Abuaf et al.[2] provide a detailed description of the TBC application process. Watt et al. focused on the boundary-layer characteristics and losses caused by the TBC layer, and Abuaf et al. studied the stagnation heat transfer on cylindrical leading-edge models coated with real TBC.

The leading-edge region of the turbine airfoil has been the focus of several heat transfer studies. O'Brien and Van Fossen[3] and Morehouse and Simoneau[4] studied the effects of freestream turbulence on the forward half of a circular cylinder. Ota and Kon,[5,6] Bellows and Mayle,[7] and Mehendale et al.[8] studied heat transfer on a simulated semicircular leading edge with a flat afterbody. They reported that an increase in freestream turbulence intensity increases leading-edge heat transfer significantly. All of the preceding studies were for a surface without roughness or coating.

Seban,[9] Yamamoto et al.,[10] Chyu and Goldstein,[11] and Metzger et al.[12] studied heat transfer for flow over rectangular cavities on a flat surface. However, the preceding studies were not intended to simulate spallations on turbine components. Ekkad and Han[13] studied the effect of cavity shape, size, and depth on heat transfer enhancement over a flat surface. The study intended to simulate various spallation geometries to correlate the effects on heat transfer. They presented detailed heat transfer enhancement distributions for various spallation geometries

Received Dec. 22, 1997; revision received June 30, 1998; accepted for publication July 15, 1998.

*Turbine Heat Transfer Laboratory, Department of Mechanical Engineering; currently Assistant Professor, Department of Mechanical Engineering, Louisiana State University, Baton Rouge, LA 70803.

†HTRI Professor, Turbine Heat Transfer Laboratory, Department of Mechanical Engineering. Associate Fellow AIAA.

using a transient liquid-crystal technique. They reported that increases in cavity size and depth increases heat transfer enhancement because of spallation. They also reported that cavities with longer axial length produced higher heat transfer enhancement on the flat surface.

The present study simulates the effect of TBC spallation on a cylindrical leading-edge model. The spallation sizes were based on scaling from real engine spalls and TBC thicknesses from land-based gas-turbine engines. Heat transfer tests were conducted at three freestream turbulence levels for four spallation locations on the leading edge. Detailed heat transfer enhancement distributions are presented within and around the spallation. A transient liquid-crystal technique was used to obtain the detailed heat transfer distributions on the leading-edge surface. Two different spallation depths were studied at each spallation location to understand the effect of spallation depth. The high-resolution results help identify local high- and low-heat transfer regions caused by flow reattachment and separation, respectively.

Test Apparatus and Instrumentation

A schematic of the wind tunnel is shown in Fig. 1. The suction-type wind tunnel was designed to avoid uncontrolled turbulence at the inlet of the test section. A flow straightener is followed by a contraction inlet nozzle. The nozzle has a contraction ratio of 3:1. The test tunnel is 25.4 cm × 76.2 cm in cross section and 183 cm long with the cylindrical model placed 77.5 cm downstream of the nozzle exit. A tailboard was placed at the rear of the cylinder to reduce the downstream wake effects on upstream heat transfer. A grid is placed at the nozzle exit for the generation of higher freestream turbulence. The image-processing system for analyzing the liquid-crystal color changes consists of a personal computer with a color frame-grabber board, a red–green–blue (RGB) camera, a color monitor, and customized software. The color image processing system is described in detail by Ekkad et al.[14]

Two turbulence grids were fabricated to generate different levels of freestream turbulence intensity. Grid 1 is made of stainless-steel bars, is 0.5 cm square in cross section, and is 1.9 cm in pitch. Grid 2 is made of hollow brass tubes, is 1.3 cm square in cross section, and is 4.8 cm in pitch. The width and height of the grids are the same as those of the test tunnel. Both grids have an open area of 54%. The turbulence grids generate turbulence intensity levels close to actual engine conditions. Hot-wire probes were inserted through slots to measure the oncoming flow velocity and turbulent fluctuations. A calibrated single-wire probe was used to measure mainstream flow behavior. It was connected to a four-channel TSI IFA-100 hot-wire anemometer. The analog signal was digitized using a 250-kHz A/D board in a personal computer.

Figure 2 shows the cylindrical test model. The cylinder, 7.62 cm in diameter and 25.4 cm long, is hollow with six cartridge heaters embedded along the circumference to heat the outer surface uniformly. The cartridge heaters, 25.4 cm long and

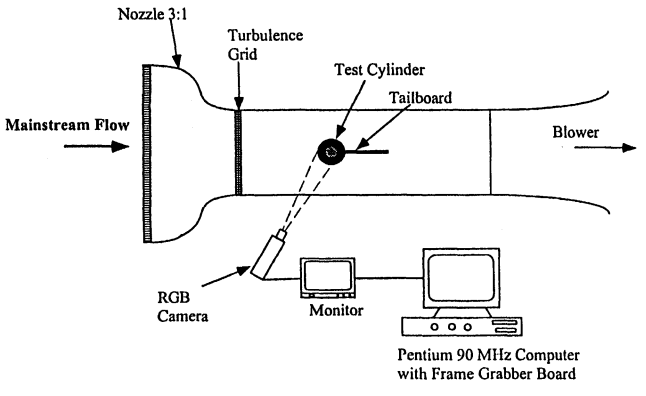

Fig. 1 Experimental setup.

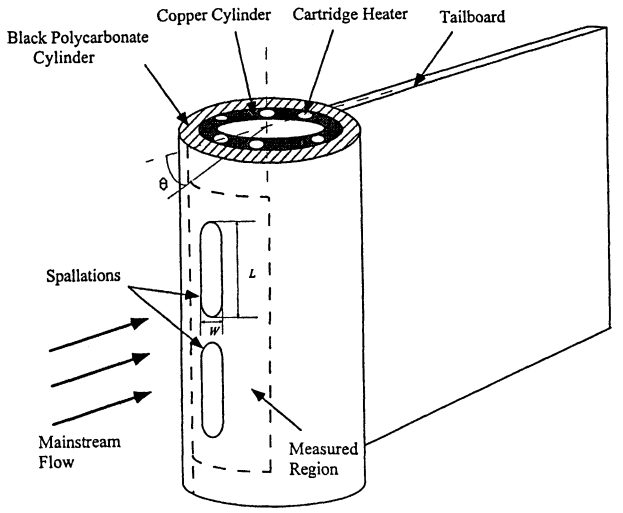

Fig. 2 Cylindrical test model with spallation.

0.32 cm in diameter, conduct to a copper cylinder that is in contact with the black polycarbonate exterior surface. There was no airspace between the polycarbonate and copper layers. The polycarbonate layer is 0.964 cm thick and has low thermal conductivity and diffusivity. The front half of the polycarbonate exterior can be changed for different spallation locations. Spallations were machined on each piece at a different location. A spallation occupies about a 20 deg width on the cylinder surface. Spallations were placed at 0–20 deg (S1), 10–30 deg (S2), 20–40 deg (S3), and 35–55 deg (S4). All of the spallations are 1.27 cm wide (W) and 3.81 cm long (L). Two different spallation depths of 0.25 and 0.51 cm were tested for each spallation location. Figure 2 also illustrates a typical spallation location on the cylinder test model. The real TBC spallation is of irregular shape and it is difficult to estimate the real effect of the spallation under actual engine conditions. The real TBC spallation is simulated as a rectangular slot with rounded edges in the present study. Also, the real engine blade TBC thickness that spalls is in the range between 5 and 20 μm. The leading-edge model in this study is about 5–10 larger scale than the actual engine blade, whereas the mainstream velocity is much lower to simulate flow Reynolds numbers around the leading-edge region of the turbine blade. Also, there is a need to also scale the spallation depth, size, and shape to simulate the actual dimensions.[13] However, the present study only compares the depth and location effects for the same spallation size and shape.

The measurement region is also indicated in Fig. 2. The measured region is limited to one side of the front half of the cylinder from stagnation (0 deg) to about 70 deg from stagnation.

Theory and Procedure

The heat transfer measurement is obtained by the transient liquid-crystal technique. The test surface is made of polycarbonate, which is a good thermal insulator. The test surface is heated to a uniform temperature using the cartridge heaters. When a uniform surface temperature is achieved, the cartridge heaters are shut off and the transient test is initiated by blowing the mainstream air over the test surface. The transient liquid-crystal technique[13,14] is a well-established technique for accurate heat transfer measurement. The surface temperature was monitored by the color image processing system. The time taken by every pixel location to change to a red color on the test surface was recorded. Local heat transfer coefficient (h) over the test surface coated with liquid crystals can be obtained by using a one-dimensional semi-infinite solid assumption on the test surface. The solution of the surface temperature re-

sponse for the one-dimensional transient conduction equation with a convective boundary condition was obtained as

$$\frac{T_w - T_i}{T_\infty - T_i} = 1 - \exp\left(\frac{h^2\alpha t}{k^2}\right)\operatorname{erfc}\left(\frac{h\sqrt{\alpha t}}{k}\right)$$

Knowing the initial temperature ($T_i \sim 40$°C) of the test surface, the mainstream temperature (T_∞), and the time of appearance of red color at every location, the local heat transfer coefficient (h) can be calculated. The liquid-crystal red appearance temperature ($T_w \sim 32.7$°C) can be obtained from in situ calibrations. The liquid-crystal color change times are typically between 10–40 s from initiation of the transient test. Here, k and α are the polycarbonate thermal conductivity and diffusivity, respectively.

The initial surface temperature of the test surface coated with liquid crystals was monitored by six thermocouples placed on the surface around the measurement region. The temperatures were within ±1°C of each other when the surface was heated to the required initial temperature. The average error in the h measurement was estimated to be about ±5.5%. The contribution to the uncertainty in heat transfer coefficient measurement was mainly from the measured color change time and surface temperature. The maximum error in measurement is typically at the edges where two-dimensional conduction occurs. In such regions, the uncertainty in measurement is around ±17%. The uncertainty in the heat transfer coefficient was estimated using the methodology of Kline and McClintock.[15]

Results and Discussion

Tests were conducted in a low-speed wind tunnel for a Reynolds number (Re) of 100,900, based on the cylinder diameter and approach velocity. Two grids were used to generate higher freestream turbulence intensity. Heat transfer tests were run at three freestream turbulence levels of 1, 4.1, and 7.1%.

Flowfield Measurements

Velocity and turbulence intensity were measured to characterize mainstream flow conditions. The leading-edge cylindrical model produced a blockage of about 12.5% of the entire width of the test tunnel. The mainstream velocity distribution during the tests was the same (±2%), regardless of the freestream turbulence conditions. Incident mainstream velocity (U_∞) was 21 m/s at $X/D = 9.5$ ($X/b = 48$ for grid 1 and $X/b = 18.5$ for grid 2) from the grid location that transforms into a mainstream $Re = 100{,}900$. Oncoming freestream turbulence intensity for the no-grid case was 1.0 and 4.1% for grid 1, and 7.1% for grid 2, based on levels at $X/D = 9.5$. Corresponding dissipation length scales at the same location for the grid-generated turbulence were estimated to be about 1.3 and 1.5 cm for grids 1 and 2, respectively.

Based on the analysis for flow around a circular cylinder,[16] the boundary-layer displacement and momentum thickness were calculated at the upstream edge of the spallation location S4 (35 deg from the leading edge). The displacement thickness to spallation depth ratios were obtained to be 0.095 and 0.048 for depths of 0.25 and 0.5 cm, respectively. Similarly, the momentum thickness to spallation depth ratios were obtained to be 0.042 and 0.021. The spallation depth modeled in this study was much larger than the local boundary-layer thickness at each location. This indicates that the boundary layer will be significantly disturbed by the spallation. This may cause strong effects on local heat transfer distributions. On the actual turbine airfoil, the boundary layer was formed at the leading edge of the airfoil. Therefore, the boundary-layer thickness will be very small compared with the actual TBC layer thickness in the near leading-edge region. The boundary-layer thicknesses to spallation depth ratios modeled in this study may be similar to that existing on actual airfoils.

Smooth Surface Heat Transfer

Heat transfer coefficient tests were run for a smooth surface at three freestream turbulence levels. The local Nusselt number is normalized by the mainstream Reynolds number to obtain the Frössling number ($Nu/Re^{0.5}$). Figure 3 presents the span-averaged Frössling number distribution for all three freestream conditions. The Frössling solution for stagnation region heat transfer for zero freestream turbulence intensity[3] is also shown for comparison. The Frössling number distribution increases with an increase in freestream turbulence intensity. There is a 50% increase with grid 2 ($Tu \approx 7.1\%$) and a 30% increase with grid 1 ($Tu \approx 4.1\%$), compared with no grid ($Tu \approx 1.0\%$) at the stagnation location.

Heat Transfer with Spallation

Figure 4 presents the detailed heat transfer distributions ($Nu/Re^{0.5}$) for all of the spallation locations at $Tu = 1\%$ and a spallation depth of 0.25 cm. From the distributions for $Tu = 1\%$ it can be observed that the spallations closer to the leading edge (S1 and S2) produce higher Nusselt numbers immediately downstream of the spallation compared to spallations farther from the leading edge (S3 and S4). The highest heat transfer region inside the spallation appears to be at different locations for each spallation location. As the spallation location moves away from the leading edge (S1 to S4), the reattachment

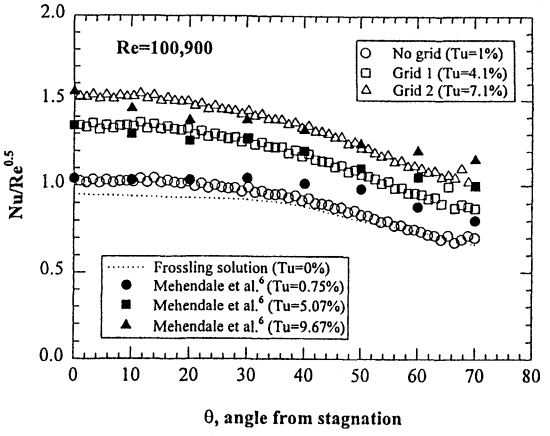

Fig. 3 Effect of freestream turbulence on smooth surface heat transfer.

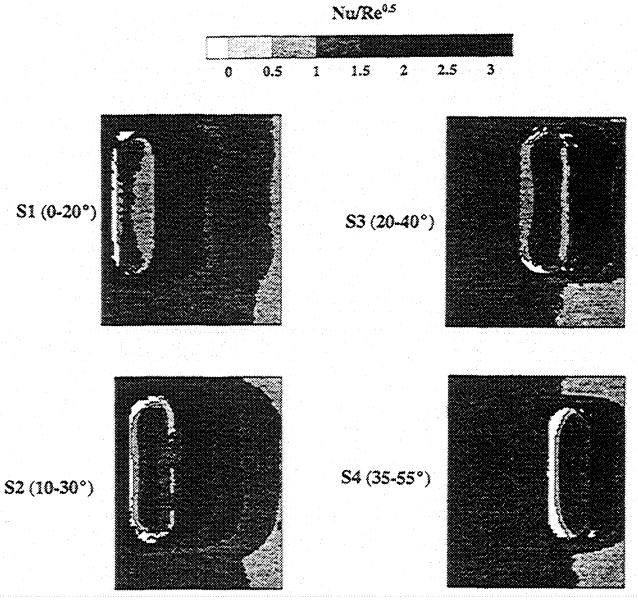

Fig. 4 Detailed heat transfer distributions for all four spallation locations for a depth of 0.25 cm and $Tu = 1\%$.

location inside the spallation appears to move closer to the downstream edge of the spallation. The detailed distributions also indicate low Nusselt numbers inside the spallation caused by the flow separation near the upstream edge of the spallation. The heat transfer distributions for higher freestream turbulence show similar trends. The detailed distributions for the spallation depth of 0.51 cm (not shown) also show similar heat transfer patterns for all four spallation locations.

Figure 5 presents the effect of freestream turbulence for each spallation location on the span-averaged Nusselt numbers ($Nu/Re^{0.5}$) for a spallation depth of 0.25 cm. The Frössling solution is also plotted for comparison. The effect of freestream turbulence is clearly evident for each spallation location. Higher freestream turbulence produces higher Nusselt numbers inside and outside the spallation. For spallations S1 and S2, the Nusselt number distributions inside the spallation show strong separation and reattachment effects. The thin boundary layer in this region may be the reason for higher Nusselt numbers downstream of the spallation for S1 and S2. Spallations S3 and S4 may be in the region where there is minimal effect on the boundary layer. However, there is strong flow separation after the upstream edge of spallation S4 that causes a very low heat transfer zone immediately inside the spallation. The flow reattached inside the spallation closer to the downstream edge, reducing the separation at the upstream edge. Note that the $Nu/Re^{0.5}$ values upstream of spallation S2 appear to be enhanced. The Nusselt numbers upstream of spallation S2 are affected by the presence of spallation S1 on the other half of the cylinder. Spallations S1 and S2 were on the same test cylinder on opposite quadrants of the cylinder. This may have caused the enhancement of Nusselt numbers upstream of spallation S2. However, in theory, spallation location is not expected to enhance upstream Nusselt numbers as clearly indicated for the S3 and S4 cases.

Figure 6 presents the effect of freestream turbulence for each spallation location on the span-averaged Nusselt numbers ($Nu/Re^{0.5}$) for a spallation depth of 0.51 cm. The Frössling solution is also plotted for comparison. The effect of freestream turbulence is clearly evident for each spallation location. Higher freestream turbulence produces higher Nusselt numbers inside and outside the spallation, as in the case for a depth of 0.25 cm. For this case, spallations S1 and S2 do not produce strong increases in Nusselt numbers downstream of the spallation. The Nusselt numbers inside and outside the spallations are nearly the same. However, spallations S3 and S4 produce strong variations inside and outside the spallations. There is flow separation after the upstream edges of spallations S3 and S4, which causes low heat transfer zones immediately inside the spallation. However, in this case, spallation S3 has slight variations inside the spallations because of freestream turbulence effects. The location of flow reattachment inside the spallation appears to be different for different freestream turbulence levels. The flow fluctuations in the mainstream could affect the reattachment location, adding to the already strong effect of curvature at this location.

Figure 7 presents the effect of depth on span-averaged heat transfer enhancement (Nu/Nu_0) at Tu = 1% for all four spallation locations. The local Nusselt number (Nu) with spallation

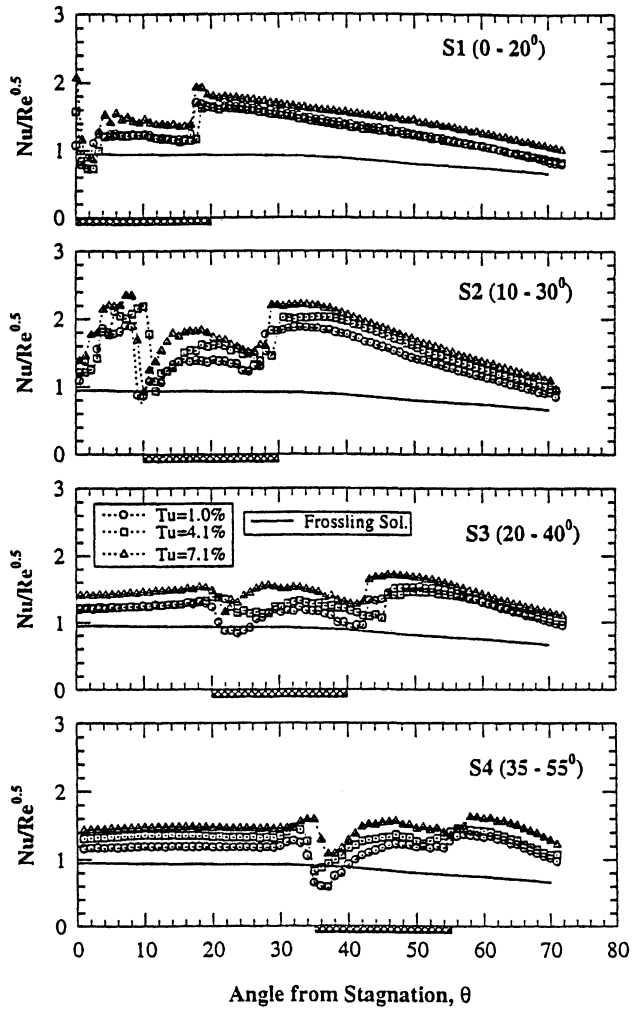

Fig. 5 Effect of freestream turbulence on span-averaged Nusselt numbers for a depth of 0.25 cm.

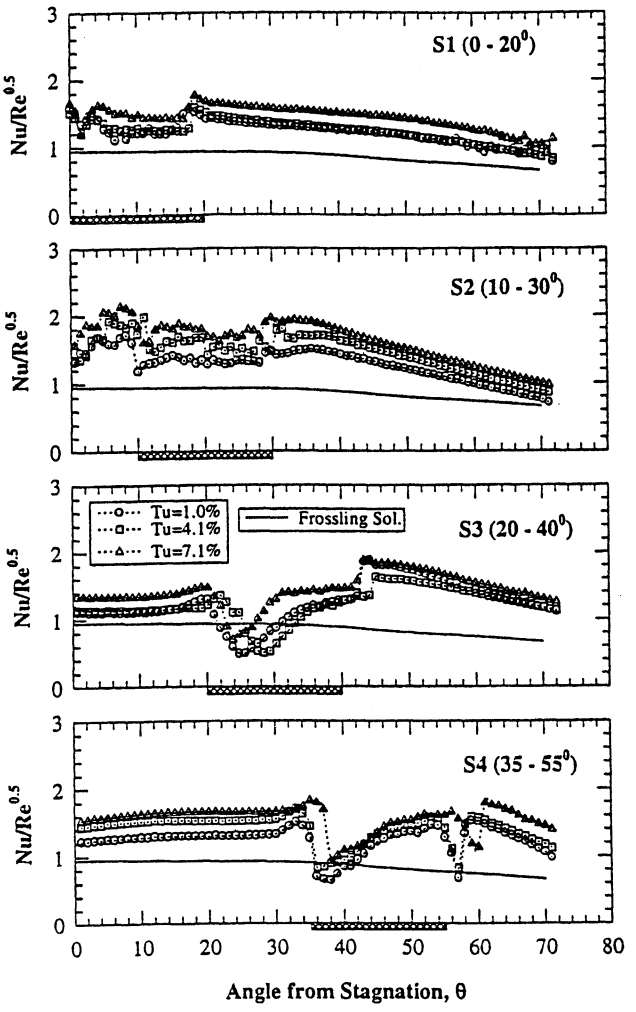

Fig. 6 Effect of freestream turbulence on span-averaged Nusselt numbers for a depth of 0.51 cm.

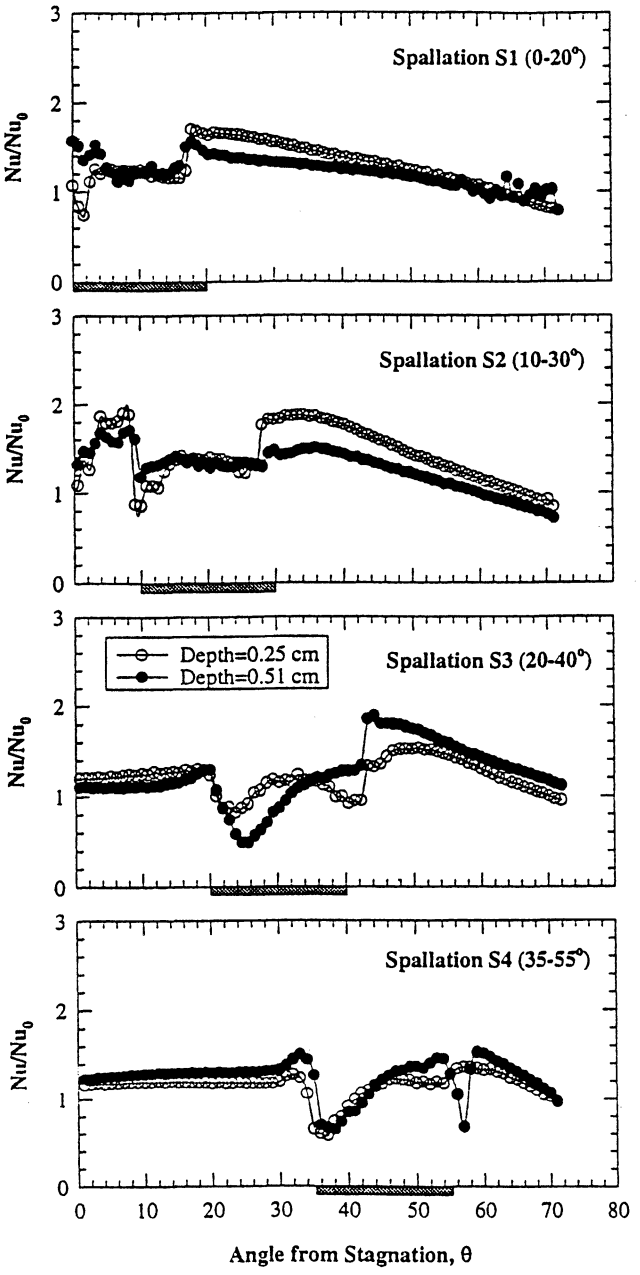

Fig. 7 Effect of spallation depth on heat transfer enhancement for Tu = 1.0%.

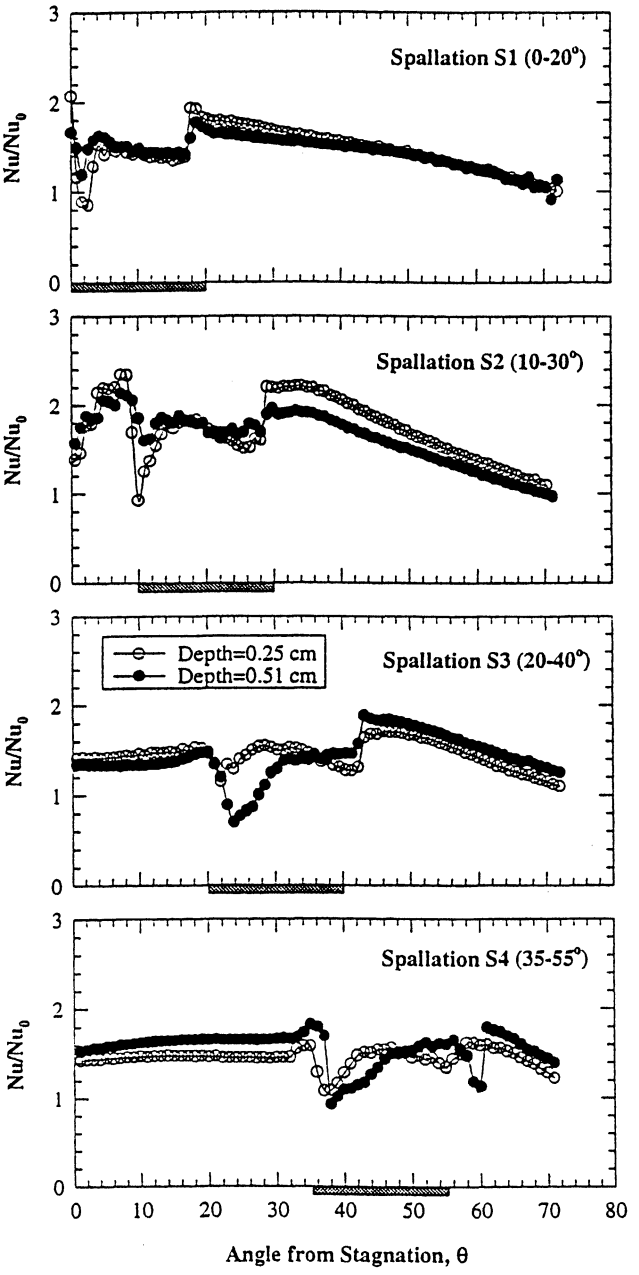

Fig. 8 Effect of spallation depth on heat transfer enhancement for Tu = 7.1%.

is normalized by the local Nusselt number for a smooth surface (Nu_0) at the same location. From the figure, it is evident that the increase in depth from 0.25 to 0.51 cm affects the heat transfer enhancement immediately downstream of the spallation for all spallation locations. For spallations S1 and S2, an increase in depth decreases heat transfer enhancement immediately downstream of the spallation. Farther downstream, the effect reduces. However, Nusselt numbers downstream of spallation are enhanced with an increase in depth for S3 and S4. This may be a result of the thicker boundary layer away from the leading edge. For spallations close to the leading edge, as in S1 and S2, the effect of depth on heat transfer enhancement inside the spallation is not very strong. However, the effect of depth inside the spallation is strong for location S3. The increase in depth changes the flow reattachment location inside the spallation. This causes the heat transfer distribution to vary inside the spallation.

Figure 8 presents the effect of spallation depth for each spallation location at Tu = 7.1%. The distributions are similar to the case at Tu = 1%. Spallation S1 shows a lesser effect of depth at Tu = 7.1%. The distributions for S2 are similar to that for low turbulence. Spallations S3 and S4 show different flow reattachment locations inside the spallation for different depths. The highly turbulent freestream affects the flow reattachment inside the spallation, causing slight variations in the heat transfer enhancement distributions inside the spallation. However, the flow separation near the downstream tip of the spallation is not affected strongly by the oncoming freestream turbulence.

Figure 9 presents regionally averaged heat transfer enhancement results for each spallation at Tu = 1 and 7.1%. Nusselt number ratios inside the spallation and one spallation distance downstream of the spallation are averaged to obtain the regionally averaged Nusselt number ratios. The regionally averaged values are plotted against spallation locations for inside and outside the spallation. For Tu = 1.0%, higher heat transfer enhancement is obtained for spallations S1 and S2 inside the spallation. Downstream of spallation, the ratio values increase

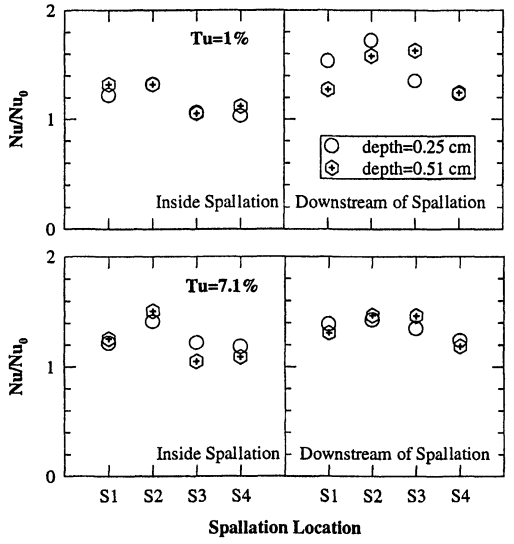

Fig. 9 Effect of spallation location, depth, and freestream turbulence intensity on regionally averaged Nusselt number ratios.

as the spallation location moves downstream from S1 and S2, and then decreases as the spallation location moves to S4. This indicates that heat transfer enhancement peaks for downstream locations of spallation S2. Highest enhancement values obtained are 1.35 for inside the spallation and 1.7 for downstream of spallation for location S2. Spallation depth has little effect on the heat transfer enhancement inside the spallation. The depth effect downstream of spallation is stronger only for spallations closer to the leading edge (S1, S2, and S3).

For $Tu = 7.1\%$, highest Nusselt number enhancement values inside the spallation are obtained for spallation S2. The effect of depth inside each spallation location is very small. Downstream of the spallation, spallation S2 produces the highest enhancement. Nusselt number enhancement levels are similar for inside and outside the spallation for a higher turbulence intensity of $Tu = 7.1\%$. Spallation S4 provides the lowest Nusselt number ratio values inside and outside the spallation. The effect of depth is insignificant on the downstream heat transfer enhancement for all spallation locations.

It is evident that the leading-edge boundary layer is most disturbed by the spallation location just downstream of the leading edge. Farther downstream, the effect of a spallation is reduced. A thinner boundary layer is affected significantly in the region of 10–30 deg downstream of the leading-edge stagnation location. This causes higher heat transfer enhancement inside and outside the spallation. Spallation depth effect is not as significant an effect as spallation location.

Conclusions

The effect of simulated TBC spallation on heat transfer distributions over a cylindrical leading-edge model has been studied using a transient liquid-crystal image method.

1) Smooth surface heat transfer is greatly enhanced by the addition of freestream turbulence. There is a 50% enhancement for a freestream turbulence of 7.1% compared with that for 1.0%.

2) Detailed heat transfer distributions for various spallation locations on the leading-edge model have been presented. Spallation location has a strong effect on local heat transfer distributions. The detailed distributions show local high- and low-heat transfer zones. Flow separation and reattachment inside the spallation can also be identified in the detailed distributions.

3) An increase in freestream turbulence increases Nusselt numbers over the entire surface for all spallation locations. Higher freestream turbulence affects the flow reattachment location inside the spallation for spallations S3 and S4. For both spallation depths, the effect of freestream turbulence is similar. Nusselt numbers immediately downstream of spallation are enhanced up to two times because of the presence of a spallation. Nusselt numbers inside the spallation are also enhanced where flow reattaches.

4) The effect of spallation depth at each spallation was also investigated. Spallation depth affects Nusselt number enhancement immediately downstream of spallation for all locations. Depth effect is not significant inside the spallation except for a slight shift in the flow reattachment location.

5) Regionally averaged Nusselt number ratios indicate that a spallation location of 10–30 deg produces the highest enhancement for inside and downstream of the spallation. Heat transfer enhancement decreases for spallations farther downstream of the leading-edge stagnation location.

Acknowledgments

This paper was prepared with the support of the U.S. Department of Energy, Morgantown Energy Technology Center, Cooperative Agreement DE-FC21-92 MC 9061. The support of D. B. Fant and L. P. Golan, the technical team of Advanced Gas Turbine Systems Research at Clemson University, is greatly appreciated. The authors acknowledge C. Pang Lee, of General Electric Aircraft Engines, for his valuable suggestions on this project.

References

[1]Watt, R. M., Allen, J. L., Baines, N. C., Simons, J. P., and George, M., "A Study of the Effects of Thermal Barrier Coating Surface Roughness on the Boundary Layer Characteristics of Gas-Turbine Aerofoils," *Journal of Turbomachinery*, Vol. 110, No. 1, 1988, pp. 88–93.

[2]Abuaf, N., Dorri, B., Lee, C. P., and Flodman, D. A., "Stagnation Point Heat Transfer with a Thermal Barrier Coating Cylinder," American Society of Mechanical Engineers, Paper 97-GT-385, June 1997.

[3]O'Brien, J. E., and Van Fossen, G. J., "The Influence of Jet-Grid Turbulence on Heat Transfer from the Stagnation Region of a Cylinder in Crossflow," American Society of Mechanical Engineers, Paper 85-HT-58, Aug. 1985.

[4]Morehouse, K. A., and Simoneau, R. J., "Effect of a Rotor Wake on the Local Heat Transfer on the Forward Half of a Circular Cylinder," *Proceedings of the International Heat Transfer Conference* (San Francisco, CA), Hemisphere, New York, 1986, pp. 1249–1255.

[5]Ota, T., and Kon, N., "Heat Transfer in the Separated and Reattached Flow on a Blunt Flat Plate," *Journal of Heat Transfer*, Vol. 96, No. 2, 1974, pp. 459–462.

[6]Ota, T., and Kon, N., "Turbulent Transfer of Momentum and Heat in a Separating and Reattaching Flow over a Blunt Flat Plate," *Journal of Heat Transfer*, Vol. 102, No. 3, 1980, pp. 749–754.

[7]Bellows, W. J., and Mayle, R. E., "Heat Transfer Downstream of a Leading Edge Separation Bubble," *Journal of Turbomachinery*, Vol. 108, No. 1, 1986, pp. 131–136.

[8]Mehendale, A. B., Han, J. C., and Ou, S., "Influence of High Mainstream Turbulence on Leading Edge Heat Transfer," *Journal of Heat Transfer*, Vol. 113, No. 4, 1991, pp. 843–850.

[9]Seban, R. A., "Heat Transfer and Flow in a Shallow Rectangular Cavity with Subsonic Turbulent Air Flow," *International Journal of Heat and Mass Transfer*, Vol. 8, No. 11, 1965, pp. 1353–1368.

[10]Yamamoto, H., Seki, N., and Fukusako, S., "Forced Convection Heat Transfer on Heated Bottom Surface of a Cavity," *Journal of Heat Transfer*, Vol. 101, No. 2, 1979, pp. 475–479.

[11]Chyu, M. K., and Goldstein, R. J., "Local Mass Transfer in Rectangular Cavities with Separated Turbulent Flow," 8th International Heat Transfer Conf., Paper 86-IHTC-230, Aug. 1986.

[12]Metzger, D. E., Bunker, R. S., and Chyu, M. K., "Cavity Heat Transfer on a Transverse Grooved Wall in a Narrow Flow Channel," *Journal of Heat Transfer*, Vol. 111, No. 1, 1989, pp. 73–79.

[13]Ekkad, S. V., and Han, J. C., "Heat Transfer Inside and Downstream of Cavities Using a Transient Liquid Crystal Method," *Journal of Thermophysics and Heat Transfer*, Vol. 10, No. 3, 1996, pp. 511–516.

[14]Ekkad, S. V., Han, J. C., and Du, H., "Detailed Film Cooling Measurements on a Cylindrical Leading Edge Model: Effect of Free-Stream Turbulence and Coolant Density," American Society of Mechanical Engineers, Paper 97-GT-181, June 1997.

[15]Kline, S. J. and McClintock, F. A., "Describing Uncertainties in Single-Sample Experiments," *Mechanical Engineering*, Vol. 75, No. 1, 1953, pp. 3–8.

[16]Schlichting, H., *Boundary-Layer Theory*, 7th ed., McGraw–Hill, New York, 1979, pp. 215–217.